AGU PUBLICATIONS

Geophysical Research Letters

RESEARCH LETTER

10.1002/2014GL060468

Key Points:
- Solar wind ion species are heated through magnetic reconnection at Mercury
- Planetary ion species are energized via Mercury's dawn-dusk electric field
- The number density of Na^+ in the pre-midnight plasma sheet is ~10% that of H^+

Correspondence to:
D. J. Gershman,
djgersh@umich.edu

Citation:
Gershman, D. J., J. A. Slavin, J. M. Raines, T. H. Zurbuchen, B. J. Anderson, H. Korth, D. N. Baker, and S. C. Solomon (2014), Ion kinetic properties in Mercury's pre-midnight plasma sheet, *Geophys. Res. Lett.*, *41*, 5740–5747, doi:10.1002/2014GL060468.

Received 9 MAY 2014
Accepted 18 JUN 2014
Accepted article online 21 JUN 2014
Published online 29 AUG 2014

Ion kinetic properties in Mercury's pre-midnight plasma sheet

Daniel J. Gershman[1,2], James A. Slavin[2], Jim M. Raines[2], Thomas H. Zurbuchen[2], Brian J. Anderson[3], Haje Korth[3], Daniel N. Baker[4], and Sean C. Solomon[5,6]

[1]Geospace Physics Laboratory, NASA Goddard Space Flight Center, Greenbelt, Maryland, USA, [2]Department of Atmospheric, Oceanic and Space Sciences, University of Michigan, Ann Arbor, Michigan, USA, [3]The Johns Hopkins University Applied Physics Laboratory, Laurel, Maryland, USA, [4]Laboratory for Atmospheric and Space Physics, University of Colorado, Boulder, Colorado, USA, [5]Department of Terrestrial Magnetism, Carnegie Institution of Washington, Washington, District of Columbia, USA, [6]Lamont-Doherty Earth Observatory, Columbia University, Palisades, New York, USA

Abstract With data from the Fast Imaging Plasma Spectrometer sensor on the MErcury Surface, Space ENvironment, GEochemistry, and Ranging spacecraft, we demonstrate that the average distributions for both solar wind and planetary ions in Mercury's pre-midnight plasma sheet are well-described by hot Maxwell-Boltzmann distributions. Temperatures and densities of the H^+-dominated plasma sheet, in the ranges ~1–10 cm^{-3} and ~5–30 MK, respectively, maintain thermal pressures of ~1 nPa. The dominant planetary ion, Na^+, has number densities about 10% that of H^+. Solar wind ions retain near-solar-wind abundances with respect to H^+ and exhibit mass-proportional ion temperatures, indicative of a reconnection-dominated heating in the magnetosphere. Conversely, planetary ion species are accelerated to similar average energies greater by a factor of ~1.5 than that of H^+. This energization is suggestive of acceleration in an electric potential, consistent with the presence of a strong centrifugal acceleration process in Mercury's magnetosphere.

1. Introduction

As a consequence of its interaction with the solar wind, Mercury's nightside magnetic field is stretched relative to that of the planetary dipole, forming a planetary magnetotail. As a result of dayside magnetic reconnection between the interplanetary magnetic field (IMF) and Mercury's intrinsic planetary magnetic field [*Slavin et al.*, 2009; *DiBraccio et al.*, 2013], substantial magnetic flux is convected across Mercury's polar cap toward the magnetotail, generating a dawn-dusk motional electric field. The combination of this electric field and Mercury's magnetic field results in gyro-averaged particle motion toward low nightside latitudes in the central plasma sheet. In addition to this particle drift motion, the small size of Mercury's magnetosphere relative to that of the planet and ion gyroradii [*Ogilvie et al.*, 1977] may result in highly non-adiabatic behavior of planetary ions, such as pronounced centrifugal acceleration effects [*Ip*, 1987; *Delcourt et al.*, 2002; *Raines et al.*, 2013, 2014; *Seki et al.*, 2013; *Delcourt*, 2013]. Careful study of the plasma sheet therefore provides insight into Mercury's miniature, reconnection-dominated magnetosphere.

Since its insertion into orbit about Mercury in March 2011, the MErcury Surface, Space ENvironment, GEochemistry, and Ranging (MESSENGER) spacecraft [*Solomon et al.*, 2001] has provided extensive observations of the magnetic field and plasma composition of the planet's space environment acquired by the Magnetometer (MAG) [*Anderson et al.*, 2007] instrument and the Fast Imaging Plasma Spectrometer (FIPS) [*Andrews et al.*, 2007] sensor, respectively. The spatial distribution of ions of planetary origin has been analyzed in terms of mass-per-charge (m/q) groups, including He^+ ($m/q = 4$), the O^+ group ($m/q = 14$–20), and the Na^+ group ($m/q = 21$–30) [*Zurbuchen et al.*, 2011; *Raines et al.*, 2013]. The fluxes of all ions observed by FIPS are enhanced in the pre-midnight (local times 18–24h) plasma sheet, and these ions have energies of several keV, indicating the presence of strong magnetospheric energization processes [*Raines et al.*, 2014]. Therefore, to elucidate the sources of observed planetary ions, the analysis of the kinetic properties of planetary ions is of equal importance to the analysis of their spatial distribution. Here, we investigate the structure of the velocity distribution functions of ions of both planetary origin (Na^+ group, O^+ group, He^+) and solar wind origin (H^+, He^{2+}, and $<OC>$, the averaged sum of solar-wind-borne O^{6+} and C^{5+} [*Gershman et al.*, 2012]) in Mercury's pre-midnight plasma sheet.

2. Data Selection

FIPS measures the energy per charge (E/q) of ions with m/q up to 40 amu/e between 0.046 and 13.7 keV/e in ~10 s. The ion optics on FIPS enable simultaneous imaging over a field of view (FOV) of ~1.15π sr, providing the incident directions for measured ions at an angular resolution of ~15°. Here we use data from 0.1 to 13.7 keV/e from four epochs, 17–29 November 2011, 10–27 February 2012, 30 April 2012 to 25 May 2012, and 29 July to 12 August 2012, when the spacecraft apoapsis was on the nightside of the planet. While in these orbits, MESSENGER passed through the plasma sheet at distances down the tail of ~6000 km (2–3 Mercury radii) when Mercury was near perihelion, at a heliocentric distance of ~0.35 AU. The coordinate system used here is the Mercury solar magnetospheric (MSM) system, which is centered on the internal dipole magnetic field (offset ~0.2 Mercury radii northward of the planet's center) and for which the X axis is directed toward the Sun, the Z axis is directed northward along the planet's rotational axis, and the Y axis completes the right-handed coordinate system [*Anderson et al.*, 2011].

FIPS E/q scans were considered to be inside the pre-midnight central plasma sheet when the spacecraft was inside the magnetosphere [*Winslow et al.*, 2013] for local times between 18h and 24h and within ±15° magnetic latitude and when the calculated proton plasma β, the ratio of total thermal pressure to magnetic pressure, was greater than 0.5. For each orbit, all measured events for each ion species were accumulated over these E/q scans to obtain orbit-averaged plasma sheet properties. The upstream solar wind speed was estimated from observations made ~1–2 h earlier in the magnetosheath flanks [*Gershman et al.*, 2013] The total numbers of measured events over all orbits for H^+, He^{2+}, and Na^+-group ions were sufficient to generate three-dimensional distribution functions. Other less abundant ion species have been analyzed only by their E/q distributions. As demonstrated by *Raines et al.* [2014] for both H^+ and Na^+-group ions in the cusp, accumulations of data from multiple orbits can be used to assess the average structure of three-dimensional distribution functions. To limit the effects of changing upstream conditions, we restricted accumulations of three-dimensional data to orbits for which the average upstream solar wind speed v_{sw} fell within a narrow range, i.e., 300 km/s $< v_{sw} <$ 400 km/s. Higher-cadence plasma parameters for H^+, He^{2+}, and Na^+-group ions derived from one-dimensional E/q distributions were then examined at all solar wind speeds.

3. Average Ion Kinetic Properties

Using moments calculated from orbit-averaged E/q spectra under the assumption of near isotropy and highly subsonic plasma [*Gershman et al.*, 2013], H^+ densities and temperatures were estimated for all individual MESSENGER passes through the pre-midnight plasma sheet and are shown in Figure 1a. The density and temperature ranges of the upstream solar wind [*Gershman et al.*, 2012; *Baker et al.*, 2013], subsolar magnetosheath [*Gershman et al.*, 2013], and northern magnetic cusp [*Raines et al.*, 2014] characterized over similar time ranges at Mercury are included in Figure 1a for comparison. The plasma-sheet protons maintain a thermal pressure between 0.5 and 2.0 nPa, consistent with plasma-sheet pressures derived by *Korth et al.* [2011, 2014] through analysis of diamagnetic depressions. These plasma parameters are shown as a function of their corresponding upstream solar wind velocity in Figures 1b and 1c. Lower plasma-sheet ion densities and higher plasma-sheet ion temperatures are measured during times of fast upstream solar wind. Although upstream solar wind density is not measurable with FIPS, we note that solar wind density and velocity are generally anticorrelated, and the observed trend in Figure 1b is consistent with the density of the solar wind driving the density of the plasma sheet.

The plasma densities shown in Figure 1 are of the same order as those predicted by *Mukai et al.* [2004] from an empirical scaling of values from Earth. The temperatures found here primarily correspond to their derived "cold," i.e., "non-substorm," plasma-sheet values. However, these cooler ion temperatures are still an order of magnitude larger than the electron temperatures measured by Mariner 10 [*Ogilvie et al.*, 1977], indicating that the electron contribution to the total pressure here may be neglected. Ratios of ion to electron temperature of ~6–10 are consistent with analogous observations made in Earth's plasma sheet [*Baumjohann et al.*, 1989; *Wang et al.*, 2012]. The ion temperatures measured in the plasma sheet are a factor of ~3–5 times greater than those measured in Mercury's subsolar magnetosheath (~2 MK) or magnetic cusp (~5 MK). These higher temperatures, albeit not large compared with those at Earth, nonetheless indicate the presence of a substantial heating mechanism beyond the bow shock alone, consistent with the heating associated

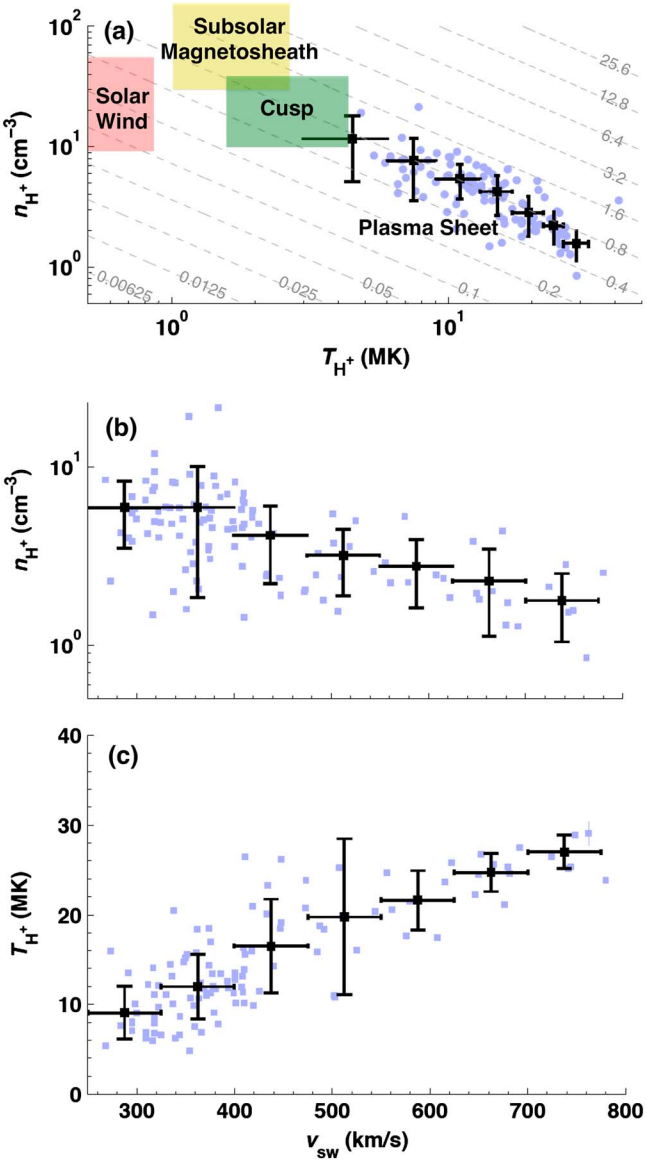

Figure 1. (a) Orbit-averaged density and temperature of H^+ in Mercury's pre-midnight/duskside plasma sheet at heliocentric distance $R \approx 0.35$ AU for 113 orbits. Lines of constant pressure (in nPa) are dashed. Ranges of H^+ density and temperature observed elsewhere in Mercury's magnetosphere are indicated with red, yellow, and green boxes for the solar wind [*Gershman et al.*, 2012; *Baker et al.*, 2013], subsolar magnetosheath [*Gershman et al.*, 2013], and northern magnetic cusp [*Raines et al.*, 2014], respectively. (b) Plasma sheet density versus upstream solar wind speed. (c) Plasma temperature versus upstream solar wind speed. Black squares denote bin averages, vertical error bars denote the standard deviation of values in each bin, and horizontal error bars correspond to the bin size.

with the high (i.e., substorm) rates of reconnection observed at Mercury compared with those at Earth [*Slavin et al.*, 2009; *DiBraccio et al.*, 2013]. *Mukai et al.* [2004] predicted that the small spatial scale of Mercury's magnetosphere may limit the maximum temperature of the central plasma sheet, but it is unlikely that the proton thermal energy would be less than the kinetic energy of the solar wind. Our findings are consistent with this assessment, with upstream solar wind speeds of ~300–800 km/s (500–3300 eV) resulting in plasma sheet proton temperatures between 5 and 30 MK (400–2600 eV).

The FIPS-measured MSM-directional fluxes averaged over all plasma sheet transits with v_{sw} between 300 and 400 km/s are shown in Figure 2 for H^+, He^{2+}, and Na^+-group ions. These fluxes, in units of cm^2 s^{-1}, are integrated over energy between 0.1 and 13.7 keV/e at an angular resolution of 20°. For each time step in the accumulation, each pixel in the FIPS detector is mapped to MSM velocity space. All measured fluxes that map to a particular MSM bin are then averaged, resulting in a directional flux map that accounts for the changes in FIPS viewing geometry with time [*Raines et al.*, 2014]. For these orbits, the FIPS FOV included particles with $v_{Z,MSM} > 0$. The sunward and anti-sunward directions were obscured from FIPS by portions of the MESSENGER spacecraft. Because of a direction-dependent viewing normalization, statistical counting errors can create apparent small-scale structure in the fluxes that should not be interpreted as true distribution-function structure. Larger-scale structures that span multiple angular bins, however, are resolvable by FIPS [*Raines et al.*, 2014].

For all ions in Figure 2, substantial fluxes are measured at all visible directions, indicative of hot, subsonic plasma. The H^+ and He^{2+} distributions have overall flux variations (the standard deviation divided by the average) that are less than ~15% and ~25%, respectively, with slight enhancements in dawnward ($v_{Y,MSM} < 0$) fluxes by a factor of ~1.5. The Na^+-group ions, however, show a clear factor of ~5 enhancement in duskward ($v_{Y,MSM} > 0$) fluxes, indicative of a flow of planetary ions with respect to the H^+ and He^{2+} in the

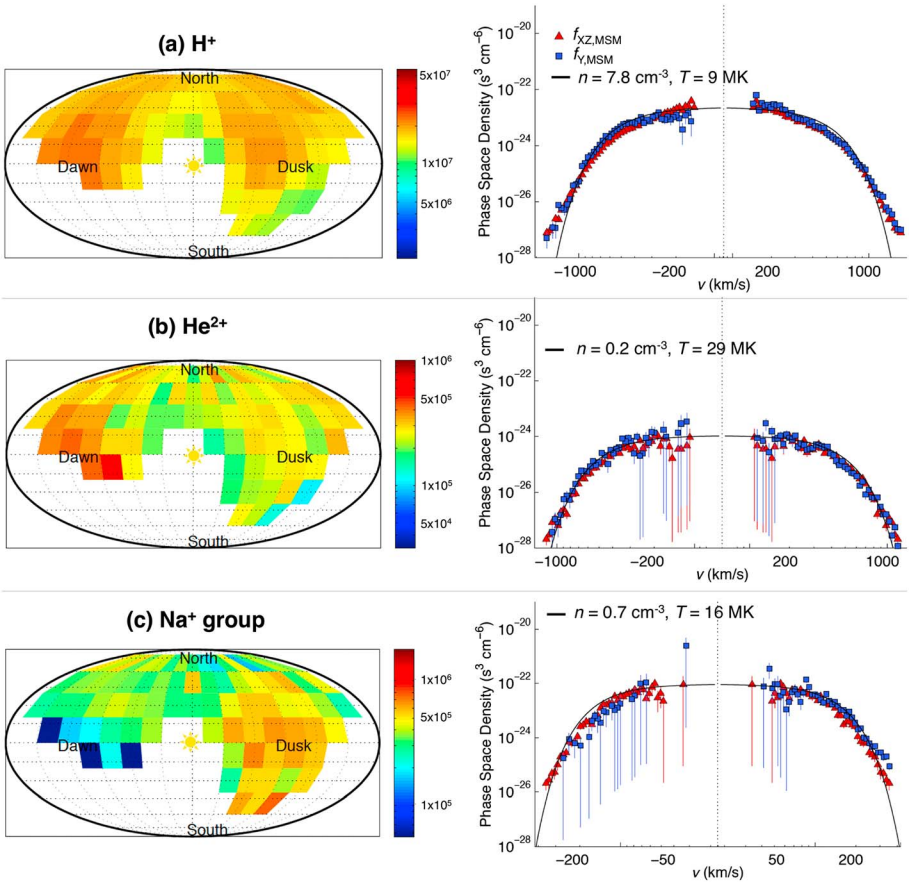

Figure 2. (Left) Map of directional fluxes ($cm^{-2}\,s^{-1}$) in MSM coordinates (see text and *Raines et al.* [2014]) and (right) phase-space distributions as a function of f_Y (blue squares) and f_{XZ} (red triangles) for (a) H^+, (b) He^{2+}, and (c) Na^+-group ions averaged over the pre-midnight plasma sheet for 300 km/s $< v_{sw} <$ 400 km/s. The color scale is logarithmic; white pixels in the flux maps indicate sections of the velocity distribution in MSM that are not visible to FIPS because of its limited FOV. The f_{XZ} distributions have been mirrored around the $v = 0$ axis. Equivalent Maxwell-Boltzmann velocity distributions derived from moments of the total accumulated *E/q* spectra are shown as solid black lines for each species.

direction of the magnetospheric electric field. To examine the energy variation of these distributions, we accumulate events in angular bins of 20° and 36° for protons and heavier ions species, respectively, to form velocity distributions parallel ($f_{Y,MSM}$) and perpendicular ($f_{XZ,MSM}$) to the positive $v_{Y,MSM}$ direction, shown in Figure 2. All distributions are highly subsonic, with $f_{Y,MSM} \sim f_{XZ,MSM}$. The Na^+-group ions show a systematic $+v_{Y,MSM}$ shift of $f_{Y,MSM}$ that is consistent with an average duskward flow speed of ~25 km/s relative to the solar wind ion species.

The average velocity distributions for all measured ions for time periods when 300 km/s $< v_{sw} <$ 400 km/s are shown in Figure 3. Under the assumption that the less abundant planetary ion species follow hot Maxwellian-like distributions similar to those of the Na^+-group ions, we can compute average ion densities and temperatures relative to those of protons ($n = 7.8\,cm^{-3}$, $T = 9.3$ MK), as shown in Figures 3b and 3c, respectively. Solar wind ions have relative abundances consistent with those of the upstream slow solar wind and exhibit near mass-proportional temperatures. The planetary ion species, however, all have average temperatures that are a factor of ~1.5 greater than that of the protons. These values imply that planetary ions could on average contribute ~15% and ~50% to the plasma thermal pressure and mass density in the pre-midnight plasma sheet, respectively.

Under the assumption of highly subsonic flow, there are a sufficient number of events to estimate the density and temperature of Na^+-group and He^{2+} ions from *E/q* spectra accumulated during individual plasma sheet passes. The temperatures of each ion are plotted as a function of the corresponding plasma sheet H^+

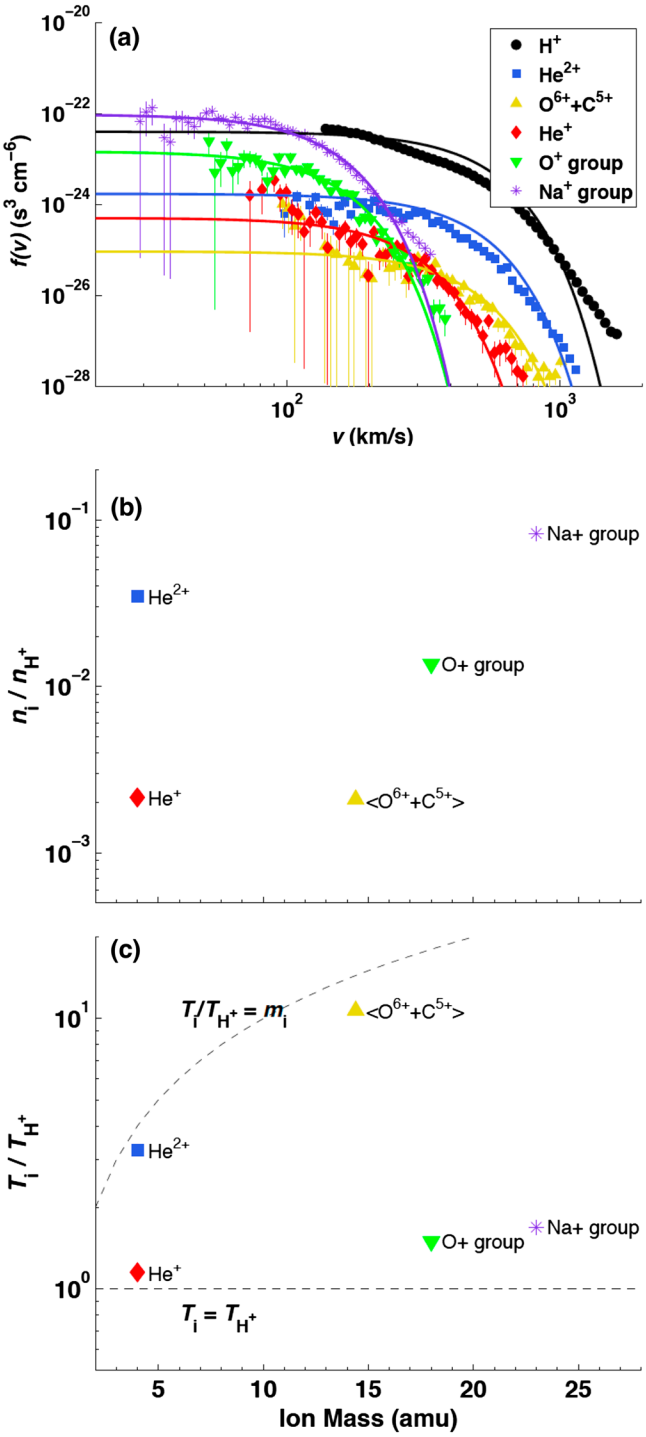

Figure 3. (a) Average $f(v)$ for six ion species measured by FIPS in the pre-midnight plasma sheet for 300 km/s $< v_{sw} <$ 400 km/s. Isotropic Maxwell-Boltzmann velocity distributions derived from moments of the accumulated E/q spectra are shown as solid lines for each species. (b) Average density of each species relative to H^+. (c) Average temperature T_i of each species relative to that of H^+. Dashed lines corresponding to $T_i = T_{H+}$ and $T_i/T_{H+} = m_i$ are also shown.

temperature in Figure 4. The temperature of He^{2+} increases linearly with that of H^+ as $T_{He^{2+}}/T_{H^+}$ ~4, consistent with mass-proportional ion heating under all solar wind conditions. The Na^+-group ion temperatures, however, rise linearly only for $T_{H^+} <$ 20 MK (i.e., $v_{sw} <$ 500 km/s) and then appear to saturate at ~30 MK for $T_{H^+} >$ 20 MK (i.e., $v_{sw} >$ 500 km/s).

4. Discussion

The high temperatures of solar wind ion species in the plasma sheet compared with those observed in the subsolar magnetosheath and cusp, as well as their mass-proportional temperatures, are consistent with all solar wind ion species being heated to the same thermal velocities of ~200–500 km/s, a range similar to that expected for reconnection outflow speeds (i.e., the local Alfvén speeds) in the nightside plasma sheet. Given the large inferred reconnection rates [*Slavin et al.*, 2009; *DiBraccio et al.*, 2013], we conclude that magnetic reconnection, both on the dayside and in the magnetotail, is the dominant process of solar wind ion energization within Mercury's plasma sheet. The initial entry of solar wind plasma into the magnetosphere may be a consequence of both dayside magnetic reconnection and Kelvin-Helmholtz vortices on the magnetopause flanks [*Sundberg et al.*, 2012; *Korth et al.*, 2014]. Although the relative contribution of plasma entry between these two mechanisms is unknown, it is likely that the large reconnection rates at Mercury observed for all IMF conditions [*DiBraccio et al.*, 2013; *Gershman et al.*, 2013] inhibit the formation of the type of super-dense, cold plasma sheet that forms at the Earth in the absence of strong tail reconnection [*Thomsen et al.*, 2003].

The observed spatial distributions of planetary ions [*Raines et al.*, 2013] combined with the kinetic properties presented here result in three main conclusions. First, because ions with m/q ratios between 4 amu/e and

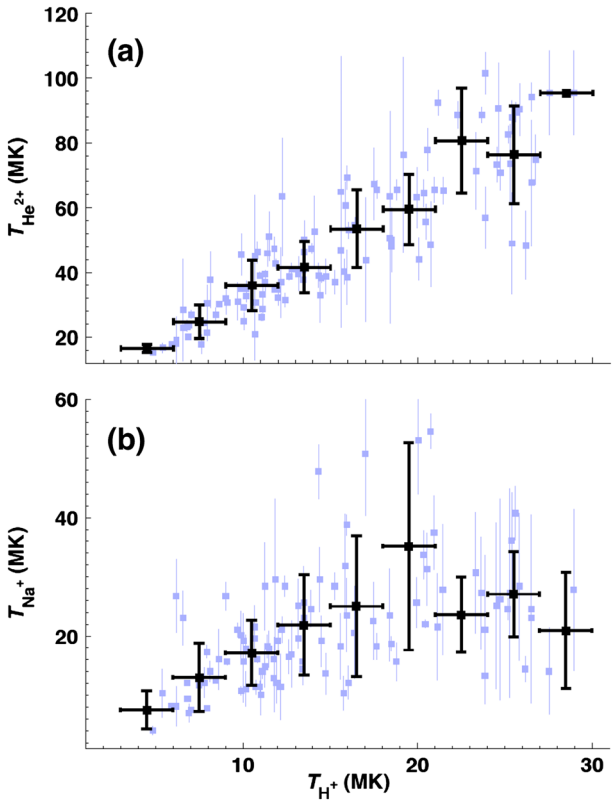

Figure 4. Pre-midnight plasma sheet temperatures of (a) He^{2+} and (b) Na^+-group ions as a function of T_{H+}. The individual uncertainties reported here correspond to counting error effects on the recovery of plasma parameters as described by *Gershman et al.* [2013]. Black squares denote bin averages, vertical error bars correspond to the standard deviation of values in each bin, and horizontal error bars correspond to the bin size.

$m/q = 23$ amu/e vary in average energy by less than a factor of 2, accelerated He^+, O^+-group, and Na^+-group ions observed in the plasma sheet must follow similar trajectories, undergoing acceleration in a dawn-dusk electric field. Second, ions must either originate from a broad source region or undergo substantial wave-particle scattering in order to achieve an apparent near-thermal distribution. Finally, solar wind ion species (m/q ~1–3 amu/e) are not strongly influenced by these processes.

Because heavy solar wind ions have m/q ratios near that of He^+ but show different behavior, it is likely that keV-energy planetary plasma sheet ions originate inside Mercury's magnetosphere at low energies, rather than being picked up to higher initial energies in the magnetosheath or upstream from the bow shock. Centrifugal acceleration, studied in detail at Mercury by *Delcourt et al.* [2002, 2003], *Delcourt* [2013], and *Seki et al.* [2013], is the most likely candidate for such an energization process, through which ions with large gyroradii are subjected to centrifugal acceleration on field lines that convect over the polar cap by magnetospheric $\mathbf{E} \times \mathbf{B}$ drift (where **E** and **B** are the local electric and magnetic fields, respectively) and subsequently thermalize in the pre-midnight plasma sheet. This transport of planetary ions from Mercury's polar regions into the magnetotail is analogous to ionospheric outflow of O^+ ions at Earth that achieve keV energies in the plasma sheet, where they can dominate the local energy density [*Lennartsson and Shelley*, 1986; *Kistler et al.*, 2006; *Mouikis et al.*, 2010]. In order for their trajectories to be bounded within the magnetosphere, ions must originate with low energies (<10 eV). We expect that all planetary ion species will likely have broad dayside and/or cusp source regions of such low-energy ions [*Raines et al.*, 2013, 2014]. Centrifugal acceleration of these ions should result in trajectories that are not strong functions of their m/q [*Delcourt*, 2013], enabling enhanced fluxes of all ion species to be observed in the pre-midnight sheet with similar energies. Some m/q dependence on energy may be a result of finite gyroradius interactions with the magnetotail current sheet [*Delcourt*, 2013]. The observed saturation in ion temperatures at ~30 MK for $v_{sw} > 500$ km/s could be a result of loss of higher-energy ions with large gyroradii in the dayside magnetosphere during times of compressed magnetospheric geometry, or it could indicate an upper limit to the strength of Mercury's dawn-dusk electric field.

Although planetary ions are present in sufficient numbers to contribute to both the plasma thermal pressure and mass density, it is not clear to what degree the motion of the heavy planetary ions corresponds to adiabatic magnetohydrodynamic convection. On the basis of a comparison of ion gyroradii at keV energies and predicted field line curvature, Na^+ ions should have quasi-adiabatic orbits in the tail [*Delcourt et al.*, 2003], though such trajectories are difficult to characterize with observations from only a single spacecraft. Finally, although magnetic turbulent power has been observed to maximize in the high-β plasma sheet [*Uritsky et al.*, 2011; *Boardsen et al.*, 2012], no conclusive evidence has been reported for the presence in these regions of

Na^+-generated ion-cyclotron waves that would enable substantial wave-particle scattering of planetary ions into increasingly thermal distributions.

5. Conclusions

The far-tail plasma sheet at Mercury is populated by hot ions of both solar wind and planetary origin. The solar wind ions maintain their ion composition, exhibit a factor of ~5 heating over that observed in the subsolar magnetosheath, and have mass-proportional temperatures, consistent with a reconnection-dominated energization within Mercury's magnetospheric system. Planetary ions, however, with a wide range of *m/q* ratios (4–23 amu/e), are all accelerated to energies that are a factor of ~1.5 greater than that of the protons, and Na^+ temperatures saturate at ~30 MK for $v_{sw} > 500$ km/s. These ions observed in the pre-midnight plasma sheet likely originate from inside Mercury's magnetosphere and are accelerated via non-adiabatic motion in Mercury's dawn-dusk electric field. They are concentrated toward the dusk-side magnetopause and are present in sufficient numbers to potentially mass-load Mercury's magnetospheric dynamics, though whether these ions are truly exhibiting collective behavior in the plasma sheet is still an open question.

Acknowledgments

The MESSENGER project is supported by the NASA Discovery Program under contracts NAS5-97271 to The Johns Hopkins University Applied Physics Laboratory and NASW-00002 to the Carnegie Institution of Washington. DJG is supported at Goddard Space Flight Center by an appointment to the NASA Postdoctoral Program administered by Oak Ridge Associated Universities. Data used in this study are available from the Planetary Data System.

The Editor thanks two anonymous reviewers for assistance in evaluating this manuscript.

References

Anderson, B. J., et al. (2007), The Magnetometer instrument on MESSENGER, *Space Sci. Rev.*, *131*, 417–450, doi:10.1007/s11214-007-9246-7.

Anderson, B. J., C. L. Johnson, H. Korth, M. E. Purucker, R. M. Winslow, J. A. Slavin, S. C. Solomon, R. L. McNutt Jr., J. M. Raines, and T. H. Zurbuchen (2011), The global magnetic field of Mercury from MESSENGER orbital observations, *Science*, *333*, 1859–1862, doi:10.1126/science.1211001.

Andrews, G. B., et al. (2007), The Energetic Particle and Plasma Spectrometer instrument on the MESSENGER spacecraft, *Space Sci. Rev.*, *131*, 523–556, doi:10.1007/s11214-007-9272-5.

Baker, D. N., et al. (2013), Solar wind forcing at Mercury: WSA-ENLIL model results, *J. Geophys. Res. Space Physics*, *118*, 45–57, doi:10.1029/2012JA018064.

Baumjohann, W., G. Paschmann, and C. A. Cattell (1989), Average plasma properties in the central plasma sheet, *J. Geophys. Res.*, *94*, 6597–6606, doi:10.1029/Ja094ia06p06597.

Boardsen, S. A., J. A. Slavin, B. J. Anderson, H. Korth, D. Schriver, and S. C. Solomon (2012), Survey of coherent ~1 Hz waves in Mercury's inner magnetosphere from MESSENGER observations, *J. Geophys. Res.*, *117*, A00M05, doi:10.1029/2012JA017822.

Delcourt, D. C. (2013), On the supply of heavy planetary material to the magnetotail of Mercury, *Ann. Geophys.*, *31*, 163–1679.

Delcourt, D. C., T. E. Moore, S. Orsini, A. Millilo, and J.-A. Sauvaud (2002), Centrifugal acceleration of ions near Mercury, *Geophys. Res. Lett.*, *29*(12), 1591, doi:10.1029/2001GL013829.

Delcourt, D. C., S. Grimald, F. Leblanc, J.-J. Berthelier, A. Millilo, A. Mura, S. Orsini, and T. E. Moore (2003), A quantitative model of the planetary Na^+ contribution to Mercury's magnetosphere, *Ann. Geophys.*, *21*, 1723–1736.

DiBraccio, G. A., J. A. Slavin, S. A. Boardsen, B. J. Anderson, H. Korth, T. H. Zurbuchen, J. M. Raines, D. N. Baker, R. L. McNutt Jr., and S. C. Solomon (2013), MESSENGER observations of magnetopause structure and dynamics at Mercury, *J. Geophys. Res. Space Physics*, *118*, 997–1008, doi:10.1002/jgra.50123.

Gershman, D. J., T. H. Zurbuchen, L. A. Fisk, J. A. Gilbert, J. M. Raines, B. J. Anderson, C. W. Smith, H. Korth, and S. C. Solomon (2012), Solar wind alpha particles and heavy ions in the inner heliosphere observed with MESSENGER, *J. Geophys. Res.*, *117*, A00M02, doi:10.1029/2012JA017829.

Gershman, D. J., J. A. Slavin, J. M. Raines, T. H. Zurbuchen, B. J. Anderson, H. Korth, D. N. Baker, and S. C. Solomon (2013), Magnetic flux pile-up and plasma depletion in Mercury's subsolar magnetosheath, *J. Geophys. Res. Space Physics*, *118*, 7181–7199, doi:10.1002/2013JA019244.

Ip, W.-H. (1987), Dynamics of electrons and heavy ions in Mercury's magnetosphere, *Icarus*, *71*, 441–447.

Kistler, L. M., et al. (2006), Ion composition and pressure changes in storm time and nonstorm substorms in the vicinity of the near-Earth neutral line, *J. Geophys. Res.*, *111*, A11222, doi:10.1029/2006JA011939.

Korth, H., B. J. Anderson, J. M. Raines, J. A. Slavin, T. H. Zurbuchen, C. L. Johnson, M. E. Purucker, R. M. Winslow, S. C. Solomon, and R. L. McNutt Jr. (2011), Plasma pressure in Mercury's equatorial magnetosphere derived from MESSENGER Magnetometer observations, *Geophys. Res. Lett.*, *38*, L22201, doi:10.1029/2011GL049451.

Korth, H., B. J. Anderson, D. J. Gershman, J. M. Raines, J. A. Slavin, T. H. Zurbuchen, S. C. Solomon, and R. L. McNutt Jr. (2014), Plasma distribution in Mercury's magnetosphere derived from MESSENGER Magnetometer and Fast Imaging Plasma Spectrometer observations, *J. Geophys. Res. Space Physics*, *119*, 2917–2932, doi:10.1002/2013JA019567.

Lennartsson, W., and E. G. Shelley (1986), Survey of 0.1 to 16 keV plasma sheet ion composition, *J. Geophys. Res.*, *91*, 3061–3076, doi:10.1029/JA091iA03p03061.

Mouikis, C. G., L. M. Kistler, Y. H. Liu, B. Klecker, A. Korth, and I. Dandouras (2010), H^+ and O^+ content of the plasma sheet at 15–19 Re as a function of geomagnetic and solar activity, *J. Geophys. Res.*, *115*, A00J16, doi:10.1029/2010JA015978.

Mukai, T., K. Ogasawara, and Y. Saito (2004), An empirical model of the plasma environment around Mercury, *Adv. Space Res.*, *33*, 2166–2171.

Ogilvie, K. W., J. D. Scudder, V. M. Vasyliunas, R. E. Hartle, and G. L. Siscoe (1977), Observations at the planet Mercury by the Plasma Electron Experiment: Mariner 10, *J. Geophys. Res.*, *82*, 1807–1824, doi:10.1029/JA082i013p01807.

Raines, J. M., et al. (2013), Distribution and compositional variations of plasma ions in Mercury's space environment: The first three Mercury years of MESSENGER observations, *J. Geophys. Res. Space Physics*, *118*, 1604–1619, doi:10.1029/2012JA018073.

Raines, J. M., D. J. Gershman, J. A. Slavin, T. H. Zurbuchen, H. Korth, B. J. Anderson, G. Gloeckler, and S. C. Solomon (2014), Structure and dynamics of Mercury's magnetospheric cusp: MESSENGER measurements of protons and planetary ions, *J. Geophys. Res. Space Physics*, doi:10.1002/2014JA020120.

Seki, K., N. Terada, M. Yagi, D. C. Delcourt, F. LeBlanc, and T. Ogino (2013), Effects of the surface conductivity and the IMF strength on the dynamics of planetary ions in Mercury's magnetosphere, *J. Geophys. Res. Space Physics*, *118*, 3233–3242, doi:10.1002/jgra.50181.

Slavin, J. A., et al. (2009), MESSENGER observations of magnetic reconnection in Mercury's magnetosphere, *Science*, *324*, 606–610, doi:10.1126/science.1172011.

Solomon, S. C., et al. (2001), The MESSENGER mission to Mercury: Scientific objectives and implementation, *Planet. Space Sci.*, *49*, 1445–1465.

Sundberg, T., S. A. Boardsen, J. A. Slavin, B. J. Anderson, H. Korth, T. H. Zurbuchen, J. M. Raines, and S. C. Solomon (2012), MESSENGER orbital observations of large-amplitude Kelvin-Helmholtz waves at Mercury's magnetopause, *J. Geophys. Res.*, *117,* A04216, doi:10.1029/2011JA017268.

Thomsen, M. F., J. E. Borovsky, R. M. Skoug, and C. W. Smith (2003), Delivery of cold, dense plasma sheet material into the near-Earth region, *J. Geophys. Res.*, *108*, 1151, doi:10.1029/2002JA009544.

Uritsky, V. M., J. A. Slavin, G. V. Khazanov, E. F. Donovan, S. A. Boardsen, B. J. Anderson, and H. Korth (2011), Kinetic-scale magnetic turbulence and finite Larmor radius effects at Mercury, *J. Geophys. Res.*, *116,* A09236, doi:10.1029/2011JA016744.

Wang, C.-P., M. Gkioulidou, L. R. Lyons, and V. Angelopoulos (2012), Spatial distributions of the ion to electron temperature ratio in the magnetosheath and plasma sheet, *J. Geophys. Res.*, *117*, A08215, doi:10.1029/2012JA017658.

Winslow, R. M., B. J. Anderson, C. L. Johnson, J. A. Slavin, H. Korth, M. E. Purucker, D. N. Baker, and S. C. Solomon (2013), Mercury's magnetopause and bow shock from MESSENGER Magnetometer observations, *J. Geophys. Res. Space Physics*, *118*, 2213–2227, doi:10.1002/jgra.50237.

Zurbuchen, T. H., et al. (2011), MESSENGER observations of the spatial distribution of planetary ions near Mercury, *Science*, *333*, 1862–1865, doi:10.1126/science.1211302.